Feasibility Study on Thickness Measurement of Coated ZrO_2 Using Optical Coherence Tomography

Jinjian Li[1], Yaoyu Ding[1,*], Tianyi Zhao[1], Chenguang Lei[1], and Libing Bai[1]
[1]School of Automation Engineering, University of Electronic Science and Technology of China, Chengdu 611731, China
202122280421@std.uestc.edu.cn, yding@uestc.edu.cn, 202121060307@std.uestc.edu.cn,592149779lcg@gmail.com
libing.bai@uestc.edu.cn
*corresponding author

Abstract—ZrO_2 is coated on nuclear fuel rod to protect it from high temperature steam oxidation and erosion, the degeneracy of the coated ZrO_2 is inevitable and needs to be measured in-situ periodically to ensure a qualified performance and meet the safety standard. The existing magnet-based method involves complex calibration procedure, which is sensitive to the radiation of the environment, and the sensor module can hardly be placed in the tiny gap between array of the fuel rods. Here, we demonstrated an extended industrial application of 1310 nm wavelength-based spectral domain optical coherence tomography for the non-destructive in-situ thickness measurement of the aforementioned ZrO_2 materials coated on the fuel rod. The nature of optical fiber overcomes the aforementioned challenges for magnet-based methods. The acquired data show a high signal to noise ratio and distinct difference between different thickness, and thus confirms the potential applicability of optical coherence tomography for in-situ thickness measurement of coated ZrO_2 materials.

Keywords-Coated ZrO_2;Thickness;Non-Destructive;Optical Coherence Tomography(OCT)

1. INTRODUCTION

ZrO_2 coating process on nuclear fuel rod has been widely used to cover the base material and protect it from damages of erosion, heat, and mechanical force in the nuclear energy industries[1-4]. Degeneracy of the coated ZrO_2 thickness is inevitable during the service, especially in harsh environment such as high temperature, high radiation, and with flow of acid liquid. The in-situ measurement of the coating thickness is mandatory to ensure a qualified performance and safety standard, and keep the costs under control[5]. Typically, non-destructive techniques are used for in-situ measurements of the coated ZrO_2 thickness, which includes X-ray Fluorescence Spectroscopy(XRF)[6],[7],ElectronProbeMicroanalysis(EPMA)[8], [9], [10], Ellipsometry[11], [12], Rutherford backscattering spectroscopy(RBS)[13], [14], and Resonant Methods[15], [16], [17]. But for a in-situ thickness measurement, the fuel rods are immersed in hot water with radiation, and they are typically assembled as a honeycomb structure with gap less than 2mm [Figure 1]. Most of the aforementioned method fail to reach the measuring surface and isolate the measurement procedure from the effect of the high temperature and radiation.

Figure 1. The fuel rod assembly

The most commonly used method for evaluating the thickness of coated ZrO_2 is electromagnetic radiation, which determines the thickness by exploiting the resonance frequencies using both microwaves [18] and visible light [19], [20]. But the calibration process is complicated and the measurements are sensitive to the radiation and environment temperature. Hence, the necessity for devising a non-destructive in-situ inspection technique for measurement of coated ZrO_2 thickness, which could isolate the measurement from the effect of the harsh environment, and be small enough to reach the measuring surface, has gained remarkable attention.

Optical Coherence Tomography (OCT) is an optical medical imaging technique [21], [22], which was recently employed in diverse defect-inspection applications as a powerful inspection tool for industrial products owing to its high resolution (on the order of microns) and non-destructive imaging capability. Reinforced from the high axial and spatial resolution of OCT, numerous studies on disease diagnosis and clinical management of tooth by OCT have been reported in the literature [23], [24], [25]. OCT has been widely used to image the cross-section of tooth for evaluation of dental caries, tooth crack, and age-related changes in tooth structure, in which the main chemical component is ZrO_2. Hence, OCT is a potential solution for in-situ thickness measurement of coated ZrO_2 material. The extra benefit of OCT system is that it delivers the detecting beam to the measuring surface though optical fiber. Given a radiation-proof optical fiber, the whole measurement process would be isolated from the effect of radiation and water, which would solve the most challenging issue during the thickness in-situ measurement for the coated ZrO_2 on fuel rod. On the other hand, the focusing lens of OCT could be integrated to the end of fiber, hence the end-detector could be as small as 1 mm, which is well suited for being flexibly located in the honeycomb structure of the fuel rod array. Hence, OCT is a potential solution for in-situ thickness measurement of coated ZrO_2 material.

979-8-3503-0247-9/23/$31.00 ©2023 IEEE
DOI 10.1109/ISSSR58837.2023.00017

In the study proposed here, we demonstrated an OCT based thickness measurement method for coated ZrO_2 materials on fuel rods to quantitatively investigate the material loss after a certain period of service. The primary focus of the study was to evaluate the measurement capability of OCT in terms of Signal to Noise Ratio (SNR), Precision, Measurement Range, and compare it with the industrial requirement. SD-OCT system were built and used to acquire A-scan depth profiles for ZrO_2 coated sample with different thickness. Algorithm for detecting the interface between the ZrO_2 and base material were developed and evaluated. The main conceptual breakthrough of this study is expanding the industrial application of OCT system from qualitatively defect detection and analysis to quantitative thickness measurement. The results provided an elaborate performance evaluation of the thickness measurement of coated ZrO_2, which suggests that OCT holds a great potential for application in the coated ZrO_2 thickness measurement.

2. SYSTEM OF SD-OCT

2.1. Theory

In a SD-OCT system, a low-coherent light is directed into a 2x2 fiberoptic couple implementing a simple Michelson interferometer, with electric field expressed in complex form $E_i = s(k,\omega)e^{i(kz-\omega t)}$. The coupler splits the light into sample and reference arms. Light exiting the reference fiber is incident upon a mirror and redirected back into the same fiber with electric field $E_R = (E_i/\sqrt{2})r_R e^{i2kz_R}$. Light exiting the sample fiber is incident upon an optical subsystem designed to focus the beam on the sample. The light backscattered or reflected from the sample with electric field $E_S = (E_i/\sqrt{2})\sum_{n=1}^{N} r_{S_n} e^{i2kz_{S_n}}$ is redirected through the same sample arm fiber, where it is mixed with the returning reference arm light in the fiber coupler, and the combined light is made to interfere on the surface of a photoreceiver. The returning fields generates a photocurrent proportional to the square of the sum of the fields incident upon it, given by

$$I_D(k,\omega) = (\rho/2)\langle|E_R + E_S|^2\rangle$$
$$= \frac{\rho}{4}\left[S(k)\left[R_{\mathrm{R}} + R_{S_1} + R_{S_2} + \cdots\right]\right]$$
$$+\frac{\rho}{2}\left[S(k)\sum_{n=1}^{N}\sqrt{R_{\mathrm{R}}R_{S_{\mathrm{n}}}}(\cos\left[2k(z_R - z_{S_n})\right])\right]$$
$$+\frac{\rho}{4}\left[S(k)\sum_{n\neq m=1}^{N}\sqrt{R_{S_{\mathrm{m}}}R_{S_{\mathrm{n}}}}(\cos\left[2k(z_{S_{\mathrm{n}}} - z_{S_m})\right])\right]$$

The electronic signals detected at the photoreceivers are processed into an A-scan, representing the depth-resolved reflectivity profile of the sample. The sample reflectivity profile $r_S(z_S) = \sqrt{R_S(z_S)}$ is estimated from the inverse Fourier transform of $I_D(k)$,which is referred to as the "A-scan":

$$i_D(z) = \frac{\rho}{8}[\gamma(z)[R_{\mathrm{R}} + R_{S_1} + R_{S_2} + \cdots]]$$
$$+\frac{\rho}{4}\sum_{n=1}^{N}\sqrt{R_{\mathrm{R}}R_{S_{\mathrm{n}}}}\left[\gamma\left[2(z_R - z_{S_n})\right] + \gamma\left[-2(z_R - z_{S_n})\right]\right] \quad \text{Cross-correlation term}$$
$$+\frac{\rho}{8}\sum_{n\neq m=1}^{N}\sqrt{R_{S_{\mathrm{m}}}R_{S_{\mathrm{n}}}}\left[\gamma\left[2(z_{S_n} - z_{S_m})\right] + \gamma\left[-2(z_{S_n} - z_{S_m})\right]\right]$$

As can be seen, the desired sample field reflectivity profile $\sqrt{R_S(z_S)} = \sum_{n=1}^{N}\sqrt{R_{S_n}}\,\delta[(z_S - z_{S_n})]$ is reproduced in the cross-correlation term.

2.2. System

The system [Figure 2] mainly consists of four arms from a 50:50 fiber optic coupler (TN1360R5A2; Thorlabs, Inc., Newton, NJ). The light source (SLD) is a fiber pigtailed SLD with close-loop thermoelectric cooling and measured to have a center wavelength of 1310 nm and a full width at a half maximum bandwidth of 42 nm. The spectrometer is based on a CMOS sensor array consisting of 1x2048 pixel array with a A-scan line rate 100kHz. A MEMS scanner is embedded in the focusing box to scan the beam in one or two directions for imaging transversely. The use of the two liquid lens in sample and reference arm, respectively, enable focusing at multiple depths without having to adjust imaging optics. The OCT software is a custom Windows application written in C++ and Qt, the main OCT algorithm (Dispersion compensation, Inverse FFT, Windowing) are computed parallelly in a GPU (GeForce RTX 3090).

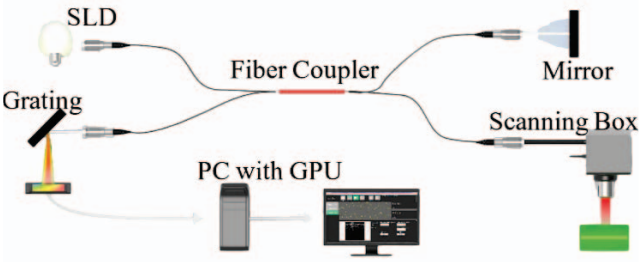

Figure 2. Schematic of the proposed SD OCT system

2.3. Material and Test Method

ZrO_2 coated rod samples [Figure 3] with five thicknesses (0um, 5um, 15um, 30um, 45um) coated by coating process-1 and two thicknesses (30um, 45um) coated by coating process-2 [Figure 3] were measured with a static beam dot on the surface of the rod bar at the focused plane of the measuring beam. 500 A-scan data were captured and post-processed for individual samples. Figure 4 show the raw interference pattern of the sample 1 to sample 5 which shows significant difference in spectrum domain.

Figure 3. ZrO_2 coated rod samples: the ones labeled 1,2,3,4,5 are 0 um, 5 um, 15 um, 30 um, 45 um thick and coated with process-1 and the ones labeled 6,7 are 30 um, 45 um thick and coated with coating process-2

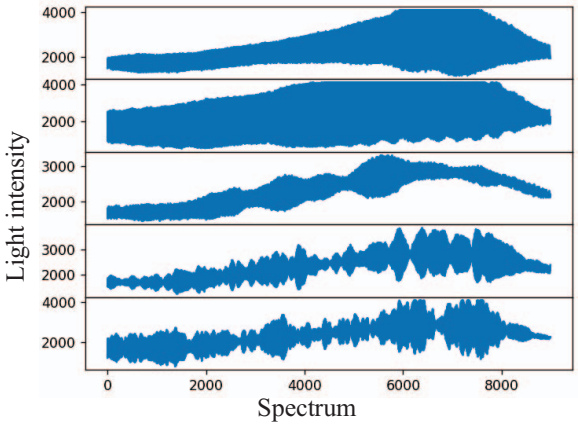

Figure 4. Raw data of the interference pattern of the 5 thicknesses coated by coating process-1

3. Thickness Measurement

The interference pattern captured in the spectrometer needs to be processed to get the depth profiles by following the steps of k-linearization, dispersion compensation, inverse FFT, and windowing. The interference patterns collected by the camera are sampled with equal wavelength increment while the inverse FFT takes wave number as input, hence, the k-linearization is conducted to sample spectrum evenly in wave number by translating the wavelength spectrum into wave number using a nonlinear scaling algorithm. The phase dispersion caused by sample material is compensated by method introduced by Maciej [28]. Finally, the depth data after inverse FFT is windowed to reduce the side lobes.

Figure 5 shows the thickness profile, which corresponds to the 7 samples labeled in Figure 3. The cake shape denotes the reflectivity of the inner structure and the depth that the probe light transmits before it hits the surface of the stainless rod which is opaque. As can been seen, they differ significantly and show great potential of measuring the thickness. The top surfaces of the cakes are distinct which are the surfaces of the coated ZrO_2, the bottoms are the boundaries between the ZrO_2 and the stainless shafts. Figure 2 shows the individual A-scan (depth profile) for the 7 samples with the beam entrance point labeled as breakpoint A and the interface between the ZrO_2 and the stainless rod labeled as breakpoint B. In order to quantitatively measure the thickness of the ZrO_2, those two points need to be determined automatically and the distance between A and B is regarded as the thickness of the measured sample of the coated ZrO_2. Algorithm was developed and detailed in the following section for detecting A and B points.

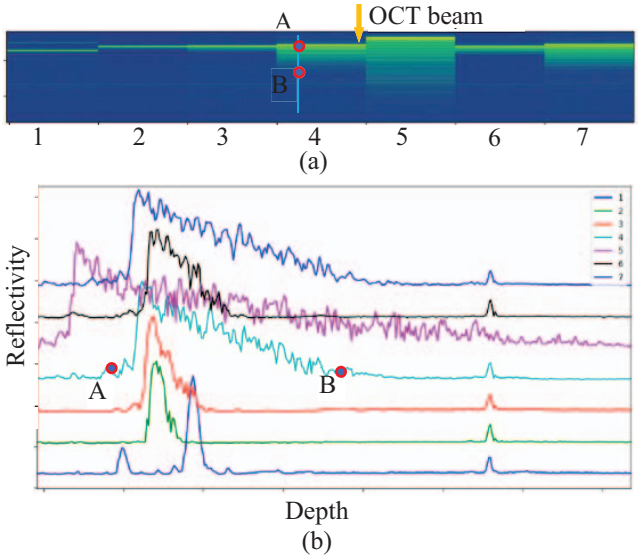

Figure 5. Depth profiles after the post processing. a: the reflectivity of the inner structure; b: the individual A-scans for the 7 samples

The A and B points were determined by the sharp change which could be calculated as standard deviation. Firstly, for each ten A-scan data, a window function was set with the length of 10-15 according to pauta criterion, which calculates the arithmetic mean x and the residual error v_i of the corresponding window each time. And then the standard deviation σ by the Besser formula was calculated. If the residual error is more than three times of σ, the outliers are removed. σ is defined as follows:

$$\sigma = [\frac{1}{n-1}\sum_{i=1}^{n} v_i{}^2]^{1/2}$$

$$= \{[\sum_{i=1}^{n} x_i{}^2 - (\sum_{i=1}^{n} x_i)^2 /n]/(n-1)\}^{1/2}$$

Then the data after the outliers been removed were averaged by ten A-scan data to reduce the noise in the direction of time. Finally, moving average by a window function was used to get the final searching result. The window size was different according to the different algorithms, and the window's step was 1 to average the original data. In the process of smoothing the mean, the abnormal data that exceeded 97% of the confidence interval after fitting the history window were removed to achieve noise reduction on the data space. 3 static window size (3,10,15) and 2 dynamic window size (5-10,3-5) were tested for searching the breakpoint A and B for measuring the thicknesses of the samples.

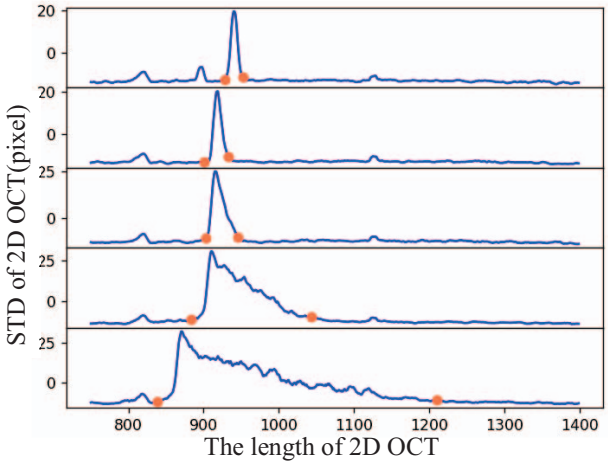

Figure 6. Schematic diagram of standard deviation and breakpoint ab calculated from raw data extracted randomly

4. Results and Analysis

4.1. Measurement Metrics

The performances of the algorithm are evaluated in terms of signal-to-noise ratio (SNR) and sensitivity, which are defined as follows:

- SNR: the ratio between the average of signal and the STD of the background noise. The formula for SNR is defined as follows:

$$SNR = \frac{AVG_{signal}}{STD_{noise}}$$

In this experiment, AVG_{signal} is defined as the identified thickness, and STD_{noise} is defined as the standard deviation of the noise.

- Sensitivity: a metric that evaluates the change of the measured result of the sensor when given a unit change on the measured object. Here, the sensitivity is defined as the measured thickness change in pixel per unit change on the real thickness of the sample. It is calculated as follows:

$$Sensitivity = \frac{P_{pixel2} - P_{pixel1}}{T_{thick2} - T_{thick1}}$$

Where P_{pixelx} is the measured thickness in pixel and T_{thickx} is the actual thickness of the corresponding sample.

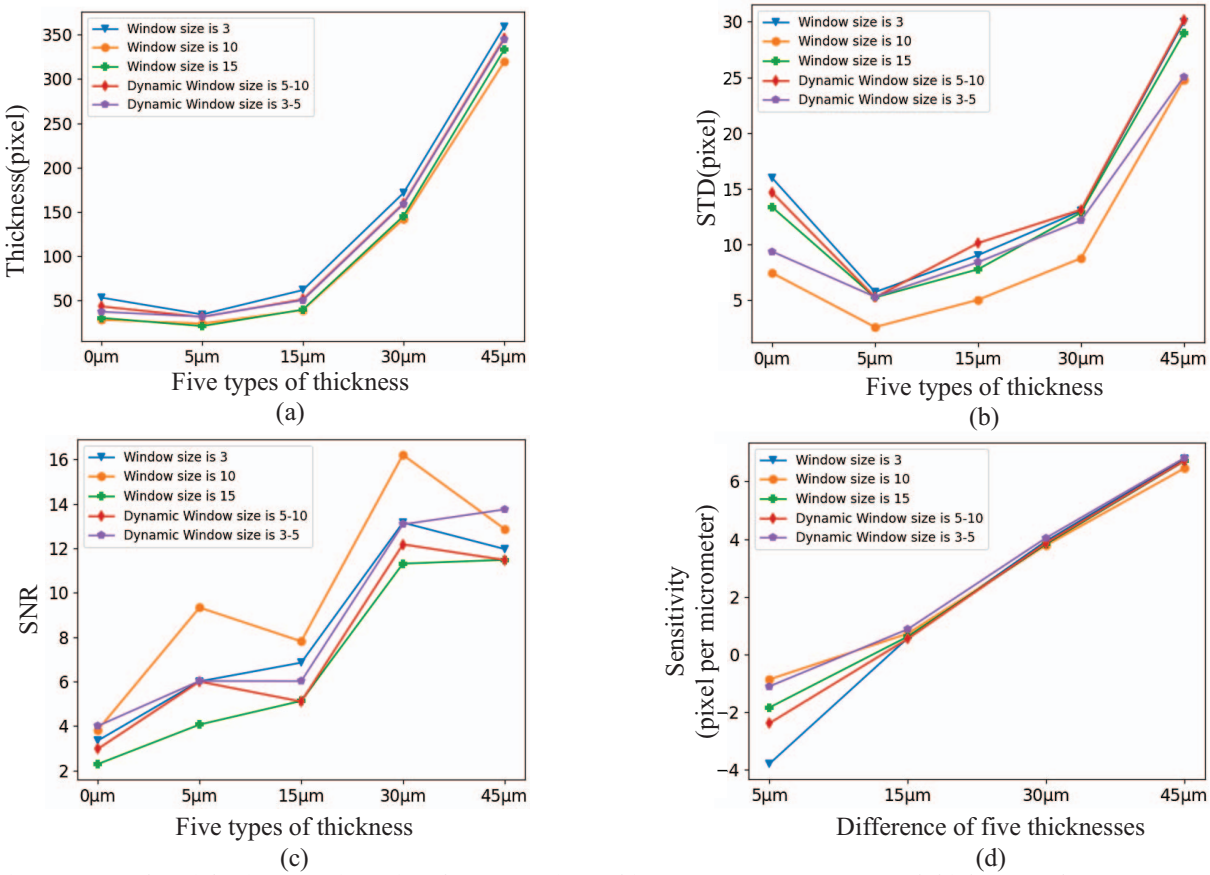

Figure 7. Results of the four metrics using the 5 sets of searching parameters. a: Averaged thicknesses; b: STD; c: SNR; d: Sensitivity

4.2. Analysis

The above five searching results were obtained by changing the size of the window in the algorithm statically and dynamically. Figure 7a shows the averaged thickness in pixel, which increases nonlinearly with the increasing of the actual thickness of the measured sample. The nonlinearity could be caused by a poor dispersion compensation which blurs the A-scan, or the un-uniformity of the coated material itself. A mapping between the pixel thickness and the physical thickness could be done by nonlinear fitting for real thickness measurement. The window size does not significantly affect the main trend on the averaged thickness. 0 um and 5 um show an abnormal trend which indicates the current imaging and postprocessing was not able to measure the thickness thinner than 5 um.

Figure 7b shows the STD of measured thickness in pixel, the measurement with higher thickness shows a higher STD, which could be caused a weakened beam after it penetrates the material. It sets a limit on the maximum thickness it can measure. The searching process with window size 10 shows the lowest STD. Figure 7c shows the SNR with different samples and windows size. The window size 10 shows the highest SNR, with most of which are great than 8, which is acceptable in the coated ZrO2 thickness measurement for fuel rod.

Figure 7d shows the sensitivity of the measurements, as can be seen, the thicker the measured object, the higher the sensitivity is, which indicates that a thickness greater than 45 um can be measured potentially. Sensitivity at 5 um thick is around 0 which means it is not able to differentiate the thickness variation thinner than 5 um. Window size doesn't significantly affect the sensitivity.

Window size 10 performs the best in terms of STD and SNR which could be adopted as the standard widow size for searching breakpoint A&B in future measurement process. With widow size 10, the measurement SNR are greater than 8 in the thickness range from 5 um to 45 um. The proposed method is not able measure the thickness less than 5 um, but it has potential to measure thickness greater than 45 um.

5. Conclusion

The utilization of micrometer resolution of OCT for the thickness measurement of coated material is a conceptual breakthrough. The aim of this study was to exploit the potential merits of OCT by quantitatively evaluating the thickness measurement performance of ZrO_2 including sensitivity, Signal to Noise Ratio, and the Measurement Range. The OCT proposed here show a great potential to quantitatively measure the thickness of the coated ZrO2 on the fuel rod. It shows the capacity of measuring thickness from 5 um to 45 um with SNR greater than 8 (precision: 12.5%), which is commonly acceptable for the thickness measurement of fuel rod. The result could be further improved by 1) conducting a series of dispersion compensation for a set of stepped thicknesses rather than just one time dispersion adopted in this research. With an auto iteration dispersion process, the boundary between the coated material and the stainless surface of the rod could be more distinct; 2) having a brighter and more focused beam which helps to penetrate deep to achieve a larger measurement range. By further minimizing the collimating and focusing module into the end of fiber, OCT could potentially play a vital role by serving as an in-situ quality assurance method of coated material with a high sensitivity as an essential tool in nuclear energy industry.

Acknowledgment

The financial support of National Natural Science Foundation of China under Grant U2030205, Grant 62003075, Grant 61903065, 62003074 and Sichuan Science and Technology Planning Project 2022JDJQ00400, 2023YFG0044 is acknowledged.

References

[1] Sawicki, Jerzy A. "Evidence of Ni2FeBO5 and m-ZrO_2 precipitates in fuel rod deposits in AOA-affected high boiling duty PWR core." Journal of Nuclear Materials 374.1-2 (2008): 248-269.

[2] Lee, Young-Ho, et al. "Role of ZrO_2 oxide layer on the fretting wear resistance of a nuclear fuel rod." Tribology International 145 (2020): 106146.

[3] Veshchunov, M. S., and A. V. Berdyshev. "Modeling of chemical interactions of fuel rod materials at high temperatures I. Simultaneous dissolution of UO2 and ZrO_2 by molten Zr in an oxidizing atmosphere." Journal of nuclear materials 252.1-2 (1998): 98-109.

[4] Sánchez-Mora, H., et al. "Nuclear fuel rod cladding oxidation and hydrogen production model based on diffusion theory in a multiphase environment of ZrO_2, α-Zr (O), and β-Zr at high temperatures (1273 K–1800 K)." International Journal of Hydrogen Energy 46.24 (2021): 13150-13161.

[5] Sawicki, Jerzy A. "Evidence of Ni2FeBO5 and m-ZrO_2 precipitates in fuel rod deposits in AOA-affected high boiling duty PWR core." Journal of Nuclear Materials 374.1-2 (2008): 248-269.

[6] Giurlani, W.; Zangari, G.; Gambinossi, F.; Passaponti, M.; Salvietti, E.; Di Benedetto, F.; Caporali, S.; Innocenti, M. Electroplating for decorative applications: Recent trends in research and development. Coatings 2018, 8, 260. [CrossRef]

[7] Innocenti, M.; Giurlani, W.; Passaponti, M.; Luca, D.; Salvietti, E. Electrodeposition and innovative characterization of precious metal alloys for the Galvanic and Jewel industry. Substantia 2019, 3, 29–37.

[8] Benoit, D.; Bresse, J.-F.; Van't dack, L.; Werner, H.; Wernisch, J. (Eds.) Microbeam and Nanobeam Analysis; Springer Vienna: Vienna, Austria, 1996; ISBN 978-3-211-82874-8.

[9] Waldo, R.A.; Militello, M.C.; Gaarenstroom, S.W. Quantitative thin-film analysis with an energy-dispersive X-ray detector. Surf. Interface Anal. 1993, 20.

[10] Gauvin, R. Quantitative X-ray microanalysis of heterogeneous materials using Monte Carlo simulations. Microchim. Acta 2006, 155.

[11] 208. Gonçalves, D.; Irene, E.A. Fundamentals and applications of spectroscopic ellipsometry. Quim. Nova 2002, 25, 794–800.

[12] Tompkins, H.; Irene, E.A. Handbook of Ellipsometry; William Andrew: Norwich, NY, USA, 2005; ISBN 9780815517474.

[13] Guimarães, Renato da S., et al. "Processing of massive Rutherford Back-scattering Spectrometry data by artificial neural networks." Nuclear Instruments and Methods in Physics Research Section B: Beam Interactions with Materials and Atoms 493 (2021): 28-34.

[14] Ager, F.J.; Respaldiza, M.A.; Botella, J.; Soares, J.C.; Da Silva, M.F.; Benítez, J.J.; Odriozola, J.A. Rutherford backscattering spectrometry (RBS) characterization of oxide scale formed on (AISI-304) steel after surface deposition of lanthanum. Acta Mater. 1996, 44, 675–681.

[15] Stachiv, I.; Kuo, C.Y.; Fang, T.H.; Mortet, V. Simultaneous determination of the residual stress, elastic modulus, density and thickness of ultrathin film utilizing vibrating doubly clamped micro-/nanobeams. AIP Adv. 2016, 6.

[16] Stachiv, I.; Zapomel, J.; Chen, Y.L. Simultaneous determination of the elastic modulus and density/thickness of ultrathin films utilizing micro-/nanoresonators under applied axial force. J. Appl. Phys. 2014, 115.

[17] Stachiv, I.; Vokoun, D.; Jeng, Y.R. Measurement of Young's modulus and volumetric mass density/thickness of ultrathin films utilizing resonant based mass sensors. Appl. Phys. Lett. 2014, 104.

[18] Lee, C.-S.; Yang, C.L. Thickness and permittivity measurement in multi-layered dielectric structures using complementary split-ring resonators. IEEE Sens. J. 2014, 14, 695–700.

[19] Wang, Q.; Li, X.; Zhao, W.M.; Jin, S. Lossy mode resonance-based fiber optic sensor using layer-by-layer SnO2 thin film and SnO2 nanoparticles. Appl. Surf. Sci. 2019, 492, 374–381.

[20] Whittaker, K.A.; Keaveney, J.; Hughes, I.G.; Sargsyan, A.; Sarkisyan, D.; Adams, C.S. Spectroscopic detection of atom-surface interactions in an atomic-vapor layer with nanoscale thickness. Phys. Rev. A At. Mol. Opt. Phys. 2015, 92, 1–11.

[21] Huang, David, et al. "Optical coherence tomography." science 254.5035 (1991): 1178-1181.

[22] Aumann, Silke, et al. "Optical coherence tomography (OCT): principle and technical realization." High resolution imaging in microscopy and ophthalmology: new frontiers in biomedical optics (2019): 59-85.

[23] Shimada, Yasushi, et al. "Evaluation of dental caries, tooth crack, and age-related changes in tooth structure using optical coherence tomography." Japanese Dental Science Review 56.1 (2020): 109-118.

[24] Bakhsh, T. A., et al. "Nondestructive evaluation of microleakage in restored primary teeth using CP-OCT." Nigerian Journal of Clinical Practice 24.6 (2021): 919-924.

[25] Kashiwa, Misa, et al. "Diagnosis of occlusal tooth wear using 3D imaging of optical coherence tomography ex vivo." Sensors 20.21 (2020): 6016.

[26] Wojtkowski, Maciej, et al. "Ultrahigh-resolution, high-speed, Fourier domain optical coherence tomography and methods for dispersion compensation." Optics express 12.11 (2004): 2404-2422